

# Multiple Ray Trace Analysis for Fast Wave Heating and Current Drive using LHD Comblin Antenna System

N. Takeuchi<sup>1)</sup>, H. Idei<sup>2)</sup>, A. Fukuyama<sup>3)</sup>, T. Seki<sup>4)</sup>, R. Kumazawa<sup>4)</sup>, T. Mutoh<sup>4)</sup>, K. Saito<sup>4)</sup>,  
H. Kasahara<sup>4)</sup>, Y. Nakamura<sup>4)</sup>, Y. Takase<sup>5)</sup>, T. Watari<sup>4)</sup>, and LHD ICRF group<sup>4)</sup>

1) Ariake National College of Technology, Omuta, Fukuoka 836-8585, Japan

2) Research Institute for Applied Mechanics, Kyushu University, Kasuga, Fukuoka 816-8580, Japan

3) Department of Nuclear Engineering, Kyoto University, Kyoto 606-8501, Japan

4) National Institute for Fusion Science, Toki, Gifu 509-5292, Japan

5) School of Science, University of Tokyo, Kashiwa, Chiba 277-8561, Japan

(Received: 3 September 2008 / Accepted: 29 May 2009)

A novel fast-wave comblin antenna was designed for use in the Large Helical Device in order to drive current in plasma, to cancel the bootstrap current, and to facilitate rotational transform profile control in high-beta experiments. The FFT  $k_{//}$ -spectrum of the fast wave “LHD comblin antenna” was calculated, and the electron power deposition profiles were evaluated by using multiple ray trace analysis in a tokamak system. The deposition profiles for each single ray in the multiple rays had a peak at  $k_{//}v_{th,e}/\omega \sim 1$  of the Doppler-shifted resonance respectively, and were summed to evaluate the weighted total deposition taking the  $k_{//}$ -spectrum into account.

Keywords : FWCD, Comblin Antenna, Multiple Ray Trace (Ray Tracing), Electron Landau Damping, ICH (ICRF), LHD, FFT, TTMP.

## 1. Introduction

Radio frequency (RF) waves and neutral beams (NB) have been used in nuclear fusion research to drive current in plasma. Many experiments have succeeded in tokamak devices when the lower hybrid current drive (LHCD) was used, however, the LHCD has a density limit and cannot drive plasma current at the center of the plasma. A fast wave current drive (FWCD) does not have such a density limit and propagates to the plasma core. Controlling the current profile using non-inductive current drive is important to plasma stability in both tokamak and helical systems. Tokamak systems need the plasma current to sustain plasma, while helical systems do not, because external helical coils provide the rotational transform. However, it is theoretically known that the self-generated bootstrap current affects plasma stability in helical systems. In the Large Helical Device (LHD), it has been proposed that the plasma current be driven in order to cancel the bootstrap current and to facilitate control of the rotational transform profile in high-beta experiments [1].

A comblin antenna has been adopted as the fast wave launcher and was set on some experimental devices for ion/electron heating and plasma current drive. It was tested on JFT-2M and TST-2. The antenna consists of some antenna elements, of which the two end elements are identical. It has some advantages over conventional loop antennas (e.g., the use of mutual coupling of a traveling wave and a wide pass-band). The comblin

antenna may excite the wave-fields with the parallel wave number  $k_{//}$ , in which the “//” subscript signifies “parallel to the magnetic field”, according to the spaces and phase-differences between the antenna elements for the current-drive experiments. The  $k_{//}$ -spectrum of the excited field was analyzed using fast Fourier transform (FFT). The deposition profiles in the LHD comblin antenna were evaluated from the multiple ray trace analysis with the  $k_{//}$ -spectrum.

This paper consists of the following sections: In Section 2, the features of a comblin antenna designed for the LHD are explained, and the  $k_{//}$ -spectrum of the antenna electric field by FFT analysis is illustrated. Section 3 describes multiple-tracing calculations, in which the values of wave numbers were collected from the antenna spectrum. In the calculation, the tokamak magnetic configuration was adopted in order to study the deposition area and velocity region in the multiple ray analysis with the  $k_{//}$ -spectrum. And in Section 4, this study is summarized and future tasks are discussed.

## 2. LHD comblin antenna

### 2.1 Comblin antenna structure

A novel comblin antenna was developed in the LHD, and the electrical properties and scenarios were studied [2-4]. The main difference between the LHD comblin antenna and other comblin antennas is that the antennas used in the experiments consist of quarter-wavelength current straps. The LHD comblin antenna, on the other hand, consists of half-wavelength current straps. It has ten

e-mail: takeuchi@ariake-nct.ac.jp

antenna elements, each of which has a T-shaped antenna strap, a back-plate, and a Faraday shield composed of 27 rods. The schematic diagram of the LHD combine antenna is shown in Fig. 1. In reality, it twists along the helical system, although it is not clear from the figure. The size of the LHD combine antenna is about 1.2 [m] (toroidal direction), 1.2 [m] (poloidal), and 0.2 [m] (major radius). The T-typed strap has two resonant modes: one is called the “even mode,” in which the current does not flow in the central support and has a constant phase in each antenna element, and another is called the “odd mode,” in which the current does flow in the central support and has reversed phase in each antenna element. Since the electric field is excited around the center of each antenna element in the even mode, the even mode is preferable to the odd mode for the fast wave current drive or electron/ion heating. The graph of the antenna’s electric field versus toroidal direction is shown in Fig. 2.

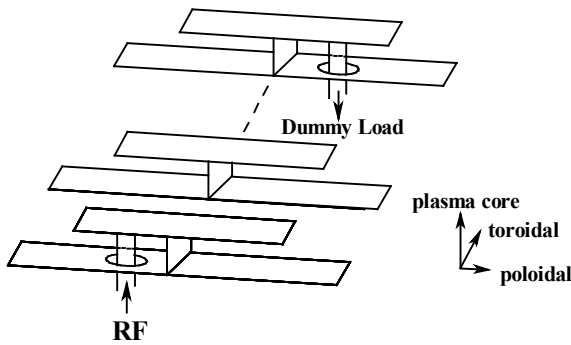


Fig.1 Schematic diagram of the LHD combine antenna.

RF is fed from one end element to the other end element, which is connected to a dummy load. The Faraday shields have been omitted from the figure. The central support has two resonant frequencies.

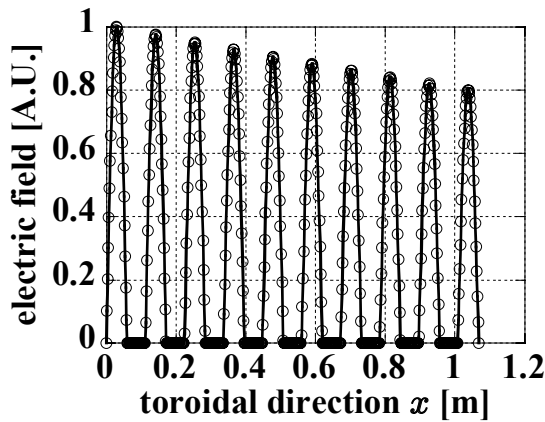


Fig.2 Profile of an electric field at the center of each antenna element for the toroidal direction. The power attenuation factor between the inlet and outlet antenna elements is assumed to be 0.8.

The phase shift between adjacent antenna elements is 0-180°, the intensity of the electric field peaks at the center of each antenna element in the toroidal direction and has a sinusoidal profile, and the power attenuation factor between the inlet and outlet of the antenna is assumed to be 0.8. The pass-band was calculated at 55-90 [MHz] and the central resonant frequency was measured in a mock-up LHD combine antenna at 75.0 [MHz] [3].

## 2.2. Parallel wave-number spectrum of the excited electric field

The spectrum and intensity of the antenna’s electric field can be calculated using FFT. The wave number structure of the combine antenna is determined based on the spacing of adjacent antenna elements and their relative phases. The power spectrum was calculated using the coupling code of an array antenna modified for the combine configuration in JFT-2M [5]. In order to calculate the  $k_{||}$ -spectrum of the excited wave-fields and check the unwanted spurious components, the excited wave was analyzed in the FFT calculation shown below. Figure 3 shows the calculated intensity of the  $k_{||}$ -spectrum (the electric field squared) excited in the LHD combine antenna at the operating frequencies of 65.7 and 75 [MHz]. There are no unwanted spurious components in the  $k_{||}$  region, indicating that effective current drive will be available using the antenna. The main  $k_{||}$  was 6.7 and 13.9 [ $m^{-1}$ ] at 65.7 and 75 [MHz]. The  $k_{||}$  with the  $-1/e$  intensity values were 3.9 and 9.8 [ $m^{-1}$ ], and 10.9 and 16.8 [ $m^{-1}$ ] at 65.7 and 75MHz, respectively. The phase differences between the antenna elements were 45° at 65.7 [MHz] while those are 90° at 75 [MHz]. This is why the excited  $k_{||}$  at 65.7 [MHz] is about half of those at 75 [MHz]. Seven rays with the main  $k_{||}$  and six  $k_{||}$  equally-separated in the  $1/e$   $k_{||}$ -width were calculated by multiple ray -tracing. The FFT intensity factor of the spectrum should be taken into account in each ray-tracing contribution. After each deposition profile is multiplied by the FFT factors, the contributions in single ray -tracing are summed in the multiple ray analysis.

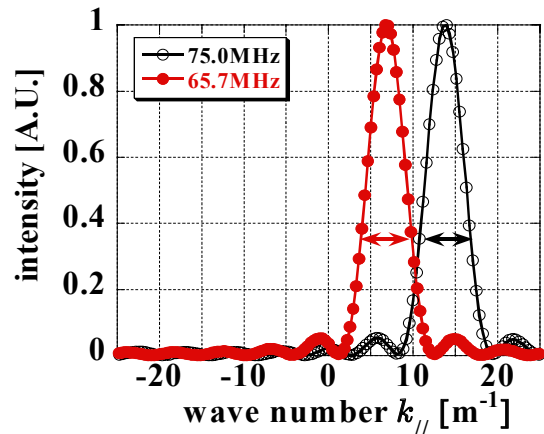


Fig.3 Intensity (the electric field squared) spectrum of antenna’s electric field

### 3. Calculations and Results

#### 3.1. Ray trace analysis

Ray tracing is a useful method for evaluating ion/electron cyclotron heating, wave damping, and current drive efficiency. The ray tracing equations are given by

$$\frac{d\vec{r}}{dt} = -\frac{\partial \text{Re}[G]}{\partial \vec{k}} \bigg/ \frac{\partial \text{Re}[G]}{\partial \omega}, \quad \frac{d\vec{k}}{dt} = \frac{\partial \text{Re}[G]}{\partial \vec{r}} \bigg/ \frac{\partial \text{Re}[G]}{\partial \omega}, \quad (1)$$

where  $\vec{r}$  is position,  $\vec{k}$  is wave number,  $\omega$  is frequency [6], and  $G$  is the dispersion relation. For fast wave, the dispersion relation can be approximated as follows:

$$\begin{aligned} G &\approx \text{Re}[G] + i(\text{Im}[G_{ion}] + \text{Im}[G_{electron}]), \\ \text{Re}[G] &= (S - N_{ij}^2)(S - N^2) - D^2 = 0, \\ \text{Im}[G_{ion}] &= \text{Im}[(K_{xx} - N_{ij}^2)(K_{xx} - N^2) + K_{xy}^2], \\ \text{Im}[G_{electron}] &= \text{Im}[G_{Landau}] + \text{Im}[G_{TTMP}] + \text{Im}[G_{cross}], \\ \text{Im}[G_{Landau}] &= \frac{N_{ij}^2 N_{\perp}^2 (S - N^2)}{|Z|^2} \frac{\omega^2}{\omega_{pe}^2 z_0} 2\sqrt{\pi} \exp(-z_0^2), \\ \text{Im}[G_{TTMP}] &= \sqrt{\pi} z_0 \beta_e N_{\perp}^2 \exp(-z_0^2) \text{Re}[(K_{xx} - N_{ij}^2)], \\ \text{Im}[G_{cross}] &= -\frac{N_{\perp}^2 \beta_e}{2} z_0 \sqrt{\pi} \exp(-z_0^2) \text{Re}[S - N_{\perp}^2], \end{aligned} \quad (2)$$

where  $N$  is refractive index,  $\omega_{pe}$  is electron plasma frequency,  $\beta_e$  is the beta value of electron, and  $S, D, K, z_0$ , and  $Z$  are Stix's notations [7]. It is noted that the last term  $\text{Im}[G_{electron}]$  includes the effect of electron Landau damping, transit time magnetic pumping (TTMP), and the cross term. The normalized energy equation is given by

$$E/E_0 = \exp\left(-2 \int (\text{Im}[G_{ion}] + \text{Im}[G_{electron}]) \bigg/ \frac{\partial \text{Re}[G]}{\partial \omega} dt\right) \quad (3)$$

where  $E$  is the energy at the ray position and  $E_0$  is that at the start point of ray tracing. The ray is traced by solving eq. (2), in which, the cold plasma dispersion  $\text{Re}[G]$  is adopted and the ion/electron cyclotron heating is calculated using the hot dispersion equation.

Although the LHD comblaine antenna was developed for the helical device, the magnetic field was given as a tokamak configuration [8] in order to study the effect of multiple ray traces and to simplify the calculation:

$$B_p(r) = \frac{B_0 a^2}{r q_a (R_0 + r \cos \theta)} \left[ 1 - \left( 1 - \frac{r^2}{a^2} \right)^\alpha \right], \quad (4)$$

where  $B_p$  is poloidal magnetic field, which is function of radius  $r$ ,  $B_0$  is toroidal magnetic field,  $R_0$  is major radius,  $a$  is plasma radius,  $\theta$  is poloidal angle,  $q_a$  is the safety factor at the plasma surface ( $r = a$ ), and  $\alpha$  is a constant obtained from an approximation of the current distribution. “ $k_{ij}$  up-shift” depends on the complex magnetic configuration in the LHD [9]. The shift affects the intensity and profile of electron damping strongly. In order to study only the difference between single- and multiple- ray tracings, we calculated ray tracings only on the tokamak system, which has a small  $k_{ij}$  shift.

The calculation parameters are  $R_0 = 3.6$  [m],  $a = 1.0$  [m],  $n_e = n_{e0}(1 - \rho^8)$ :  $n_{e0} = 2.0 \times 10^{19}$  [m<sup>-3</sup>], and  $T = T_0(1 - \rho^2)$ :  $T_0 = T_{e0} = T_{i0} = 3.0$  [keV],  $q_a = 3.0$  and  $\alpha = 3.0$ , where  $\rho$  is the normalized minor radius. The plasma

consists of electrons and hydrogen. The magnetic field  $B_0$  is 1.5 [T], where there are no fundamental/second ion cyclotron resonant layers. In such a condition, the wave energy deposits on to electrons through electron Landau damping and TTMP. If the magnetic field is set to 2.75 [T], significant ion heating is expected at the 2<sup>nd</sup> harmonic resonance layer.

#### 3.2. Calculation results

The top view of the ray trajectories for  $f = 75$  [MHz] and  $B_0 = 1.5$  [T] are shown in Fig. 4. Three typical trajectories for the main and 1/e-  $k_{ij}$  of 10.9/13.9(center)/16.8 [m<sup>-1</sup>] are drawn for only the first turn. When electron heating from the absorption of electron Landau damping and TTMP is weak, the ray should be traced for a long path-length of many turns. The rays are traced until the wave is damped to 1.0% of its initial energy. The dispersion relation,  $\text{Re}[G] = 0$ , was satisfied in the ray tracing.

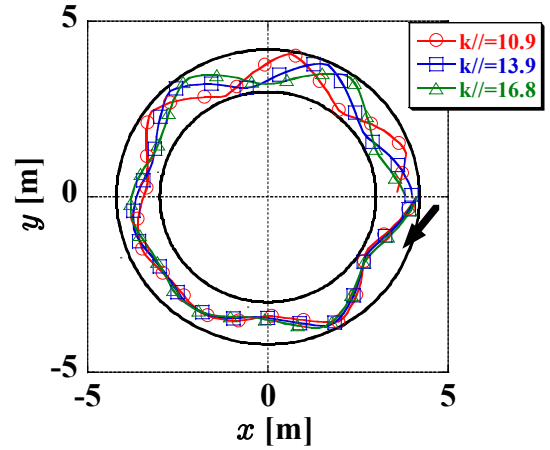


Fig.4 Top view of three typical ray trajectories ( $f=75.0$  [MHz]).

The normalized radii  $\rho$  with deposition peaks in each single ray tracing were plotted for each  $k_{ij}$  of the incident waves in Fig.5. Error bars in the obtained peak radii come from the ray step -size of each ray tracing. The peak radius results in the Doppler-shifted resonance condition of  $k_{ij}/v_{th,e} / \omega \sim 1$  in the electron Landau damping. The deposition peaks caused by the electron Landau damping disappear in the three ray calculations with lower  $k_{ij}$  for 65.7 [MHz], because the wave is well damped by TTMP. The power deposition profile in the multiple ray trace analysis is evaluated from the summation of the single ray contributions, which have different peaks with respect to each  $k_{ij}$ . The single ray contribution should be multiplied by the FFT intensity factor in the  $k_{ij}$ -spectrum. Figure 6 shows the weighted total power deposition profiles for 65.7 and 75 [MHz]. The power deposited in the outer region for 65.7 [MHz] owing to the TTMP damping is comparable to that for 75 [MHz]. Although the deposition profile in the single ray trace with the main  $k_{ij}$  has a peak due to the electron Landau damping, the profile with the lower  $k_{ij}$  in the FFT spectrum does not. The multiple ray analysis may show the effect of TTMP

with a different low value of  $k_{//}$ .

In the helical system of the LHD, it is known that the  $k_{//}$  shift occurs as the ray propagates, and the wave absorption is enhanced in the electron Landau damping. The  $k_{//}$  shift in the helical system is not emphasized in this paper. The  $k_{//}$  shift in helical devices is understood to be mainly related to the geometrical effect of the magnetic field line configuration and the dispersion effect. The amount of  $k_{//}$  shift is affected by the ray trajectory, and depends on the initial launching  $k_{//}$ . The power deposition will be evaluated in the multiple ray analysis with the  $k_{//}$ -spectrum in the helical system,

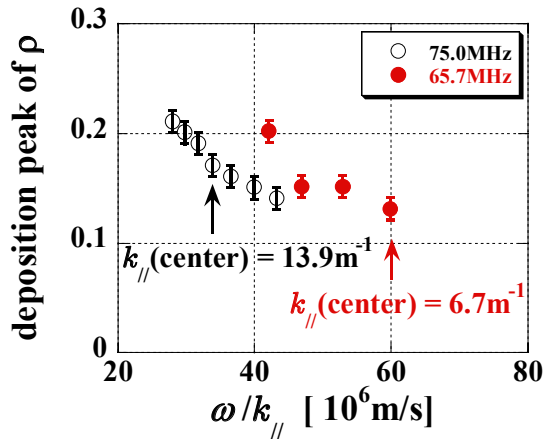


Fig.5 Deposition peaks for each  $k_{//}$  and frequency of the incident waves

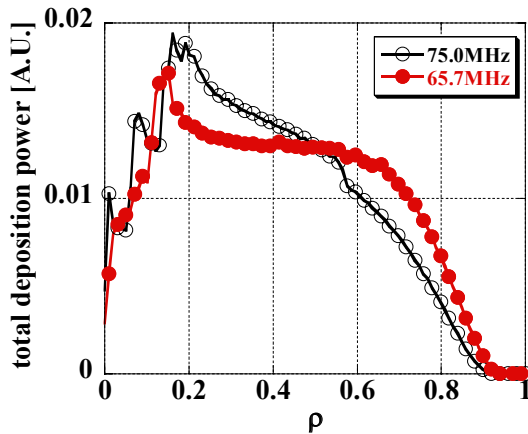


Fig.6 Total electron power deposition profile at 75 and 65.7 [MHz]. Each power is multiplied by a factor determined by the spectrum.

#### 4. Summary

The FFT  $k_{//}$ -spectrum of the fast wave “LHD comblaine antenna” was calculated for the operating frequencies of 65.7 and 75 [MHz]. There were no spurious components in the  $k_{//}$  region for either operating frequency, indicating that the effective current drive would be available using the antenna. In the multiple ray analysis with the  $k_{//}$ -spectrum, the tokamak magnetic configuration was adopted as a benchmark to study the deposition area and velocity region. The power

deposition due to electron Landau damping became strong when the Doppler-shifted resonance condition  $k_{//}v_{th,e}/\omega \sim 1$  was satisfied. The deposition profiles had different peaks depending on each launched  $k_{//}$  in the single ray tracing, but, appreciable peak disappears due to the electron Landau damping in the three ray calculations with lower  $k_{//}$  for 65.7 [MHz], because the wave was well damped by TTMP. The power deposition was evaluated from the summation of each single ray contribution. The single ray contribution should be multiplied by the FFT intensity factor in the  $k_{//}$ -spectrum. The power deposited in the outer region for 65.7 [MHz] owing to the TTMP damping was comparable to that for 75 [MHz]. The power deposition profile was controlled by excited  $k_{//}$  at the comblaine antenna. The excited  $k_{//}$  comes from the operating frequency or the phase difference between the antenna elements. The driven current profile may be controlled by the phasing of the antenna elements. In order to evaluate the driven current profile, a Fokker–Planck analysis, for instance, using TASK/FP code, should be helpful. The local wave electric field will be calculated for use in the Fokker–Planck analysis. The electron velocity distribution function distorted by the power deposition will affect the deposition itself. An iteration process in the ray trace and Fokker–Planck analyses are required. The evaluation of the driven current profile is left for future work.

The  $k_{//}$  shift in the helical system was not studied in this work. The amount of  $k_{//}$  shift is affected by the ray trajectory, and depends on the initial launching  $k_{//}$ . A three dimensional code (*e.g.*, TASK/WM) should be helpful in evaluating the detailed deposition profile or local wave field in helical systems.

#### Acknowledgement

This work was conducted as an LHD project collaboration. The authors thank members of the LHD experimental group for their continued encouragement. This work was supported in part by the Collaborative Research Program of Research Institute for Applied Mechanics, Kyushu University.

#### References

- [1] K. Ichiguchi, *et al.*, Nuclear Fusion, **33**, 481 (1993).
- [2] Y. Takase, *et al.*, Nuclear Fusion, **44**, 296 (2004).
- [3] N. Takeuchi, *et al.*, Journal of Plasma Fusion Research SERIES, **5**, 314 (2002).
- [4] N. Takeuchi, *et al.*, Fusion Science and Technology, **48**, 1267 (2005).
- [5] T. Ogawa, *et al.*, Nuclear Fusion **41**, 1767 (2001).
- [6] B. D. McVEY, Nuclear Fusion, **19**, 461 (1979).
- [7] T.H. Stix, “WAVES IN PLASMA”, AIP P7 (1992).
- [8] K. -L. Wong and M. Ono, Nuclear Fusion, **23**, 805 (1983).
- [9] N. Takeuchi, *et al.* Journal of Plasma Fusion Research SERIES, **6**, 642 (2004).